NASA Technical Memorandum 102129

Mesh Refinement in a Two-Dimensional Large Eddy Simulation of a Forced Shear Layer

R.W. Claus
Lewis Research Center
Cleveland, Ohio

P.G. Huang
Stanford University
Stanford, California

and

J.M. MacInnes
Princeton University
Princeton, New Jersey

June 1989

NASA

MESH REFINEMENT IN A TWO-DIMENSIONAL LARGE EDDY SIMULATION OF A FORCED SHEAR LAYER

R. W. Claus, NASA Lewis Research Center
P. G. Huang, Stanford University
and J. M. MacInnes, Princeton University

ABSTRACT

A series of Large Eddy Simulations are made of a forced shear layer and compared with experimental data. Several mesh densities were examined to separate the effect of numerical inaccuracy from modelling deficiencies. The turbulence model that was used to represent small scale, three-dimensional motions correctly predicted some gross features of the flow field, but appears to be structurally incorrect. The main effect of mesh refinement was to act as a "filter" on the scale of vortices that developed from the inflow boundary conditions.

INTRODUCTION

Steady-state numerical calculations of turbulent flows have been compared with experimental data for a great many years. Early on, numerical diffussion limited the validity of these comparisons and even today limits comparisons with complex three-dimensional flows. For two-dimensional problems, the improvements in numerical accuracy and the large memory capability of current computers, has allowed a fairly definitive evaluation of the validity of various turbulence models. These evaluations have illustrated several weakness of current closure models, refs. 1 and 2 for example.

There are an almost unlimited variety of approaches to improve closure models. New theoretical approaches are under study such as chaos theory. Higher moment statistical closures that attempt to introduce additional physics as for instance - multiple length scales - have been proposed and studied, ref.3. One currently popular and logical approach is to use Direct Numerical Simulations (DNS) of various flows to develop closure models. A Direct Numerical Simulation resolves all important scales of motion but these time-accurate, three-dimensional simulations are both extremely demanding of computational resources and are restricted to low Reynolds numbers. Another question concerning the utility of DNS is the universality of the turbulent structures captured in the calculation. If different structures appear in different types of flows, then an almost infinite number of simulations

must be run and a large number of closures must be developed or calibrated. If, however, there is some universitality in the calculated structures, then a closure model may be developed that is applicable to a fairly large number of flows.

One approach that relaxes this requirement for universality is Large Eddy Simulation (LES). In a Large Eddy Simulation the largest scales of turbulent motion are directly calculated (therefore are not required to be universal) and the small scales of motion are modelled. This modelling of only the small scales should make the overall closure scheme less sensitive to the geometry of the flow while greatly reducing the computational burden. But even this simplification comes close to being beyound the reach of current computer technology. If it is necessary to time-accurately calculate the development of three-dimensional structures in a flow where the mean gradients are only two-dimensional, then the computational burden remains beyound current technology, except for some idealized, simple flows. If, however, a turbulence model can be used to represent the small scale three-dimensional motions and only two-dimensional structures need to be directly calculated, then much greater predictive accuracy is available with today's computer technology. This is the main premise being examined in this paper.

In this paper a series of Large Eddy Simulations of a forced shear layer were performed to assess the predictive accuracy of a time-accurate simulation. Several mesh densities were examined to seperate the effect of numerical inaccuracy from modelling deficiencies. The forced shear layer was selected for this study due to several factors: first, the shear layer has mean gradients in only two-dimensions. It is a relatively simple geometry. The forcing dominates the early development of the layer, which, to some extent, simplifies the specification of inflow boundary conditions. Finally, the flow evolves from being completely dominated by the forced wave to a situation where the forced structure is much less significant to the development of the flow. This range of parameters is well documented in a series of experimental studies, refs. 4 and 5. This wide range of flow phenomenon makes the shear layer a good test case for schemes to improve modelling accuracy.

Computational Approach

Large Eddy Simulation

The Large Eddy Simulations (LES), performed in this report, solve the two-dimensional, Navier-Stokes equations with a two-equation turbulence model. The turbulence model is used to represent the non-periodic motion while the large scale motions are captured on a computational mesh. This methodology follows the Deardorff approach which recognizes that the solution of the discretized equations

using a finite volume algorithm is mathematically equivalent to solving the original equations with a "box" type filter, ref. 6. The advantage of this approach is that the sub-grid scale turbulence model is significantly simpified. The (Leonard) stresses that arise through the use of a more general filter (for example- a Gaussian filter) are zero. This permits the use of a turbulence model that is simply a time-dependent form of the commonly-used, Reynolds-averaged, $k-\epsilon$ model, ref.7. There are some disadvantages to this approach and reference 8 is recommended as a source detailling these issues. It is sufficient to state that, at this time, it is not clear that any significant penalties are incurred through the use of this approach.

The numerical scheme used to solve the discretized equations is an implicit, incompressible flow algorithm. Flow variables are represented on a staggered-mesh with Crank-Nicholson time differencing and QUICK differencing (ref. 9) of the convective terms. This maintains second order accuracy in both time and space. Continuity is enforced through the iterative pressure-correction scheme SIMPLE (Semi-Implicit Pressure Linked Equations), ref.10. This code is described in detail by its originators in ref. 11 and the code has undergone extensive testing and evaluation in idealized benchmark problems, ref. 12, and numerous practical flow calculations. Modifications were made to the code to improve vectorization and a more efficient solver, employing the Stone's strongly implicit algorithm combined with a block-correction, is used to solve the pressure-correction equation, ref. 13.

In applying this code to the time-dependent shear layer calculations, the domain extends from the transverse plane which is just at the trailing edge of the splitter plate (figure 1) and extends the full length of the experimental test section. Boundary conditions for u, v, k and ϵ at the inlet are prescribed according to estimates of the experimental conditions. The upper and lower boundaries were treated as imposed symmetry conditions. At the domain exit, a zero-gradient outflow boundary condition is applied to each variable. As shown in ref. 14, the use of this type of outflow boundary condition should contaminate the flow field near the outflow, but should not significantly affect the locations where the computational results are compared to experimental data.

The strongest gradients in these calculations occur in the central region of the flow domain and have a dominant y - direction component. To accomodate these gradients one-third of the mesh points in the y direction are uniformly distributed in the central 10% of the domain. The remaining two-thirds are divided among the upper and lower portions with variable spacing so that a smooth transition is made at the interface. For the finest mesh used, the streamwise X direction is resolved with 798 grid points and the Y direction with 241 points, which will be described in the abbreviated manner - 798 x 241 grid points. the grid point spacing was expanded 0.1 percent per grid cell in the axial direction. The expansion factor for the coarsest mesh calculations (150 x 80) was 0.267 percent and the expansion factor for the 400 x 241 mesh calculations was 0.2 percent. These mesh points were

distributed over a range of 0 to 2000 mm in the X direction and -200 to +200 mm in the Y direction.

The shear layer is known as a convectively unstable type of flow, ref. 15. This means that small perturbations upstream grow exponentially as they are convected with the flow. For this reason, it was recognized that the treatment of the inflow boundary condition was very important in establishing a correct comparison with experimental data. Unfortunately, detailed measurements near the splitter plate were not available so that it was neccessary to estimate the thickness of the boundary layers as they left the splitter plate. A momentum thickness (θ) estimate of 0.5 mm for the layer on each side of the splitter plate was inserted into an exponential profile:

$$u = u_\infty exp\{-(y - y_0)/2\theta\}, \qquad y_0(t) = Y sin\omega t$$

$$v = 0$$

Where the oscillation of the plate position, y_0, at the experimental frequency, ω=45 Hz, and amplitude, Y, simulates the effect of the flapping metal strip, placed at the trailing edge of the splitter plate in the experiment. The free stream velocities are 10 m/s and 6 m/s in the two separate supply streams. Numerically, a number of different inflow boundary profiles were simulated. Without examining an infinite number of permutations, the profile described here was selected as reasonably representative of experimental conditions. But it is certainly true that the calculations are very sensitive to this boundary condition and it is appropriate here to emphasize the importance of documenting the details of the inlet flow for an experiment to provide useful information for testing calculations.

Inlet conditions for the turbulence model were somewhat easier to establish. The experiment documented a streamwise turbulence intensity of around 0.2 percent, so $k \simeq \overline{u'^2} = 4x10^{-4}\ m^2/s^2$ is used. The length scale of the turbulence entering the test section was not documented, but can be estimated from the formula $\epsilon = k^{3/2}/l$ using a length scale on the order of $l \simeq 2mm$. Fortunately, some test calculations indicate that the results are not sensitive to the precise value of ϵ used, within a reasonable range.

As noted previously, these are incompressible flow calculations wherein a perturbation anywhere in the flow field can be "felt" everywhere else in the flow. Practically, what this requires is that the calculations be run for a long time period to allow the initial conditions of the flow to be completely "flushed" through the computational domain until periodic flow behavior is reached. This is partially affected by the level of mass residual allowed in the iterative calculation, where the lower the residual, the faster the approach to periodicity. The laminar flow calculations were much more sensitive to this effect and generally had to be run for longer flow times to reach periodicity.

Laminar Flow Calculations

These calculations are identical to those described above except that a constant molecular viscosity is used in place of the turbulence model viscosity. The Reynolds number, based on the mean convective velocity and the wavelength of forcing, was 9600 which is approximately an order of magnitude lower than the experimental levels.

RESULTS AND DISCUSSION

A schematic outline of the flow geometry and the main features of the forced, flow field are illustrated in figure 1. Initially the shear layer is subject to very rapid growth due to the roll-up of vortices scaling on the wavelength of the forcing. Somewhat further downstream, the roll-up process saturates and the shear layer stops growing. This is followed by a collapse of the layer width and then by a slow, secondary growth. It is in this region of slow secondary growth that the Reynolds stresses change from being "phase-locked" or dominated by the forcing wavelength to being dominated by the "random" field. In this area the phase locked stresses will exhibit negative levels while the total stresses are positive. These features of the flow field, documented in ref. 5, provide several tests for the efficacy of the numerical model.

The instantaneous vorticity for the three different mesh densities calculated are shown in figure 2. In general, the calculations display the development of both positive and negative voticity as the boundary layers leave the splitter plate and form large scale structures based on the wavelength of forcing. The positive vorticity regions (dashed contours) result from the low speed boundary layer that is used as an inflow boundary condition. These contours are rapidly dissipated when the large scale structure begins to develop. The mean flow gradient encourages the formation of negative vorticity, and the calculations indicate that this is the main component of vorticity in the flow field.

The first level of mesh refinement (going from 150 x 80 to 400 x 241 grid points - figs. 2a and 2b) smooths the development of the large, forced vortex and establishes higher levels of negative vorticity that are convected further further downstream. Further mesh refinement (fig. 2c) allows more small scale structures to form and develop immediately downstream from the splitter plate. Many of these structures are rapidly dissipated until one strong vortex and a weaker "daughter" vortex are seen around X=600 mm. The weaker vortex then merges with the stronger vortex around X= 800 to 1000 mm. This pairing phenomenon is not displayed in the coarser mesh calculations and appears to occurr mainly as a function of the near inflow mesh resolution.

The mean axial velocity thickness profiles (figure 3) are only slightly effected

by mesh resolution. The initial growth rates differ only slightly for the various calculations. Around X= 800 mm the fine mesh calculations display a thickness on the high speed side that is greater than the other calculations, due largely to the vortex pairing that occurs in this region. None of the calculations match the experimental data in detail althought they all display the same general profile. The collapse of the shear layer, shown in the mean profile for the low speed side of the shear layer around X = 600 mm, is not seen in any of the calculated profiles. In general, the calculations also do not pick up the appropriate slow secondary growth.

Despite this failure of the calculations to match the details of the mean velocity profiles, the averaged Reynolds stresses display the correct trend. The experimental stresses are initially highly positive, leading toward the growth of the layer. Later, the stresses turn negative as the shear layer collapses. Finally, the stresses become slightly positive. In the Large Eddy Simulation, this same behavior is seen in the "total" averaged Reynolds stresses displayed in figure 4. Although the location of the pockets of positive and negative stress change from one calculation to the next, they all display the same positive to negative to small positive trend. In the fine mesh calculation, the effect of vortex pairing is clearly evident around X=600 to 800 mm. The negative stresses in this region are almost completely obscured.

The total Reynolds stresses seen in figure 4 are a combination of the stresses due to the oscillatory motion (or the fluctuating structures resolved in the LES calculation) and the averaged stresses contributed by the turbulence model. The "phase locked" stresses measured in the experiment were conditionally sampled to "lock-in" on the structure produced by the forcing. These "phased locked," experimentally-measured, Reynolds stresses are equivalent to the oscillatory motion Reynolds stresses calculated from the LES.

The centerline values (Y=0 mm) of both phase locked and total stresses for both experiment and computation are shown in figure 5. In the experiment, the phased locked and total stresses coincide until after saturation of the forced structure. In the region around X=1200 -1700 mm, the phased locked and total stresses are decoupled to the extent that the total stresses are positive and the phase locked stresses are negative. The results for the medium mesh LES calculations are certainly qualitatively similar. Around X=200 to 400 mm, the Reynolds stresses are certainly dominated by the phased locked (or oscillatory) motion, although there is a discernible difference in the two stress levels. Further downstream (say around X= 1000 to 1700) the difference between the total and phase-locked stresses is more significant, due to the fact that the absolute value of the stresses is lower.

Althought there are significant differences between the LES calculation and the experimental data shown in figure 5, the overall qualitative agreement is encouraging. A forced vortex, not effected by viscosity, would nuate creating a continuous pattern of alternating positive and negative stresses as it is convected downstream. The experimental vortex is effected by the cascading process to the extent that this

nuation is damped out after the first cycle. The increased viscosity provided by the turbulence model performs similarly in the LES calculation. This provides a hint that the turbulence model may be qualitatively representing some of the effects of three dimensionality in the experiment.

A futher test of the turbulence model can be made by studying the relationship between the vortex pattern and local maxima of turbulence kinetic energy from the turbulence model. Hussain and Zaman, ref.16, have shown that the so-called random, three-dimensional, structures predominate in the braid region of the spanwise vorticities. The turbulence model used in the Large Eddy Simulation should, theoretically, represent these structures. Figure 6 displays a close-up examination of the vorticity structure superimposed upon the turbulence kinetic energy of the turbulence model for the medium mesh (400 x 241 grid points) calculation. Figure 6a is near the inflow boundary and, as such, is early in the development of the flow. In rough agreement with ref. 16, the maximum levels of turbulence kinetic energy occur in the braid regions of the flow. The levels of kinetic energy are clearly lower in the center of the vortex. Figure 6b is for the same medium mesh calculation, but is near the exit of the flow field. In this region of the flow, the maximums of kinetic energy are coincident with the centers of the vortex which clearly contradicts ref. 16. One can conjuncture that the strong forcing used in this experiment will cause the streamwise vorticies to be wrapped into the vortex core. This would lead to a local increase in turbulence kinetic energy in the core. But this seems to be more of an adhoc justification, rather than speculation supported by experimental data. The favorable results in figure 6a do not remain constant with mesh refinement. Figure 6c displays the results of the fine mesh calculation in the same approximate region of the flow as shown in figure 6a. From this figure it appears that the maximas are mostly located in or near the vortex cores. This variation with mesh refinement leads to the speculation that what is really happening early in the flow field is that the high levels in turbulence model kinetic energy that result from the extremely steep gradients early in the flow are simply convected downstream and broken-up by the vortex roll-up process. This is a strong indication that the turbulence model is not correctly representing three-dimensional structures, but rather is being convected to some of the correct portions of the flow. In the regions of the flow where the turbulence kinetic energy is being generated (further downstream) the maximas aline with the vortex cores.

While the turbulence model does not appear to be performing correctly as regards the structural details, in a gross sense the behavior is more appropriate and this can be seen in figure 7. The phased locked and the total Reynolds stresses, both computational and experimental, are shown in figure 7 for the axial location X=1700 mm. The computational phase-locked and total stresses are lower in magnitude than the experimental values, but they are correct in sign. This trend is unaffected by mesh refinement.

Figure 8 displays the instantaneous kinetic energy of the turbulence model for several different mesh densities. The highest level of turbulence model kinetic energy is near the inflow boundary where the mean velocity gradients are quite steep. These levels are dissipated further downstream until near the later portion of the flow (approximately 1600 to 2000 mm) where the turbulence kinetic energy levels begin to increase. This behavior is similar for the various mesh densiies used in the calculation, but the details vary significantly. The experiment indicates that the small-scale turbulence levels should increase in the downstream regions, so the general behavior of the calculations is encouraging. The calculations should, however, increase more rapidly in the downstream energy levels. This discrepancy is not attributable to the effects of numerical inaccuracy. The fine mesh calculation actually shows a slower increase in downstream energy levels that the medium mesh calculation. The coarse mesh calculation displays the slowest growth rate of all the calculations, but this calculation is clearly significantly effected by numerical diffusion. The medium and fine mesh calculations are also likely to be affected by numerical diffusion but not enough to alter the displayed trend.

The only other turbulence energy in these calculations is the kinetic energy of the oscillatory motion. Figure 9 displays the instantaneous kinetic energy of the oscillatory motion for the various mesh densities studied. In general, these levels are all higher than the kinetic energy contributed by the turbulence model. For example, around X= 400 mm typical levels of the oscillatory motion kinetic energy are 2.0 compared to levels of approximately 0.2 for the turbulence model. Further downstream the levels become somewhat more comparable. But whereas the levels of kinetic energy are increasing for the turbulence model far downstream, the energy in the oscillatory motion is being rapidly dissipated.

There is no uniform mesh refinement effect on the kinetic energy of the oscillatory motion. The coarse mesh calculation displays higher levels of energy further downstream than the medium mesh calculation, whereas the fine mesh calculation displays the highest levels.

The kinetic energy in the LES calculations is generated by several different sources. The kinetic energy of the random motions is represented by the k equation in the turbulence model. This equation has two generation terms. First, there is the generation of random motion kinetic energy by the mean gradient and, second, generation by the oscillatory motion gradients. The oscillatory motion kinetic energy has one primary generation term - generation by the mean velocity gradient. If one looks at all these sources as contributors to the total kinetic energy in a Large Eddy Simulation, then perhaps the magnitude of these various terms change with mesh refinement in a manner explaining the variation of results seen in figures 8 and 9.

Examining each of these generation terms indicates that the term associated with the oscillatory motion kinetic energy changes the most with mesh refinement.

Oscillatory motion gradients generate approximately twice as much random motion kinetic energy in the fine mesh calculation (798 x 241 grid points) as opposed to the coarse mesh calculation (150 x 82 grid points). Mean gradients generate half as much random motion kinetic energy in the fine mesh calculation as opposed to the coarse mesh calculation. So the random motion kinetic energy is increased by the oscillatory motion gradient and decreased by the mean gradients as the computational mesh spacing is decreased. The oscillatory motion gradients generate an order of magnitude greater contribution to the oscillatory motion kinetic energy in the fine mesh calculation as opposed to the coarse mesh. These levels are displayed in figures 10a and 10b. This variation is much greater than the variation seen in the random motion turbulence energy terms. Apparently, the mesh refinement is more effective at increasing the strength of the oscillatory motion than the random motions.

While, in general, the results of the LES calculations have been encouraging, a question naturally arises as to whether a simplier sub-grid turbulence model might not provide similar results. To examine this question a laminar calculation was made at a flow Reynolds number of 9,600. This is approximately an order of magnitude lower than in the experiment. This added viscosity is meant to represent a proscribed mixing-length, eddy viscosity concept. Figure 11 displays the vorticity and averaged Reynolds stress resulting from this calculation. Both the instantaneous vorticity and the averaged Reynolds stresses are very similar to the medium mesh calculations, fig. 3b. As in the case with the LES calculations, the added viscosity damps the nuation of the forced vortex. A laminar calculation at a Reynolds number more representative of experimental conditions (ref. 17) would not damp the nuation as quickly. Of coarse this requires that the effects of numerical diffusion be reduced to a fairly low level and the coarse mesh calculations are not sufficiently well resolved. While the eddy viscosity results appear somewhat similar to the LES calculations, the distinction between phased-locked and total stresses cannot be made. The oscillatory motion represents the only turbulence energy in this calculation. If the Reynolds stresses at X=1700 mm were plotted (as in figure 6), both the phase locked and the total stresses would be negative. But this distinction only becomes significant far downstream.

Summary

A series of Large Eddy Simulations of a forced shear flow were performed to examine the predictive accuracy of this type of computational method. Various mesh densities were used in these calculations to separate the effects of numerical inaccuracy from the effects of the turbulence model. The main effect of mesh refinement in this series of calculations was to act as a "filter" on the scale of perturbations

that enter the computational domain. The finer the mesh density, the smaller the scale of vortices that developed from the inflow boundary conditions. These smaller scale vorticities could significantly alter the downstream development of the shear layer. In the finest mesh calculation, small scale vortex pairing occurred that altered the growth of the layer locally. In fact the variation in the flow fields was great enough to limit any definitive conclusions about the predictive accuracy of the LES approach. The inflow boundary conditions were not measured and therefore had to be estimated. These estimated profiles were kept constant for all calculations, but with the differing mesh resolutions changing the scales of perturbations that developed from the boundary conditions, it is impossible to make a direct comparison with experimental results.

While the inflow boundary conditions limit any detailled comparison between calculation and experiment several general features of the calculation may be examined. The initial growth and saturation of the shear layer approximate the experimental results, but the slow secondary growth of the layer is not reproduced. The turbulence model appears incorrect structurally (i.e. the maximas of kinetic energy appear in vortex cores as opposed to in the braids), but it correctly contributes some gross features, such as the distinction between phase-locked stresses and total stresses.

Concluding Remarks

Further development of this computational approach is largely limited by a lack of very detailled experimental measurements. To be fair to the experimentalists, however, these types of measurements are very difficult. The small scales and high fluctuation amplitudes near the splitter plate make hot wire measurements quite difficult. Doubtless advances in experimental techniques will ameliorate this problem, but in the interverning time period, fully three dimensional simulations will be needed to provide a database for model improvement.

Acknowledgements

The authors are listed alphabetically. The use of the NAS Cray 2 for all of these calculations is gratefully acknowledged.

References

[1] Rodi, W.,"Examples of Turbulence-Model Applications," in Turbulence Models

and Their Applications, Volume 2, Collection de la Direction Des Etudes Et Recherches D' Electricite de France, Editions Eyrolles, 1984, pp. 297-401.

[2] Nallasamy, M.,"Turbulence Models and Their Applications to the Prediction of Internal Flows: A Review," Computers and Fluids, Vol. 15, No. 2, 1987, pp. 151-194.

[3] Kim, S.W. and Chen, C.P.,"A Multiple Time Scale Turbulence Model Based on Variable Partitioning of the Turbulent Kinetic Energy Spectrum," to appear in the Journal of Numerical Heat Transfer.

[4] Oster, D. and Wygnanski, I., Journal of Fluid Mechanics, vol. 123, Oct. 1982, pp. 91-130.

[5] Weisbrot, I., "A Highly Excited Turbulent Mixing Layer," M.S. Thesis, Tel Aviv University, Dept. of Fluid Mechanics and Heat Transfer, 1984; see also Weisbrot, I. and Wygnanski, I., "On Coherent Structures in a Highly Excited Mixing Layer," Journal of Fluid Mechanics, Vol. 195, Oct. 1988, pp. 137-160.

[6] Deardorff, J. W., "A Numerical Study of Three-Dimensional Turbulent Channel Flow at Large Reynolds Number," Journal of Fluid Mechanics, Vol. 41, 1970, pp. 452-480.

[7] Launder, B. E. and Spalding, D. B., "The Numerical Computation of Turbulent Flows," Computer Methods in Applied Mechanics and Engineering, Vol. 3, 1974, pp. 269-289.

[8] Ferziger, J. H.,"Higher level simulations of turbulent flows," Computational Methods for Turbulent, Transonic, and Viscous Flows, Hemisphere Publishing, 1983, pp. 93-182.

[9] Leonard, B. P.,"Stable and Accurate Convective Modelling Procedure Based on Quadratic Upstream Interpolation," Computer Methods in Applied Mechanics and Engineering, Vol. 19, June 1979, pp. 59-98.

[10] Patankar, S. V. and Spalding, D. B., " A Calculation Procedure for Heat, Mass and Momentum Transfer in Three-Dimensional Parabolic Flows," International Journal of Heat and Mass Transfer, Vol. 15, No. 10, Oct. 1972, pp. 1787-1806.

[11] Huang, P. G. and Leschziner, M. A.,"An Introduction and Guide to the Computer Code TEAM," Thermofluids Division technical report TFD/83/9(r), Department of Mechanical Engineering, University of Manchester Institute of Science and Technology, 1983.

[12] Huang, P. G., Launder, B. E. and Leschziner, M. A., "Discretization of Nonlinear Convection Processes: A Broad Range Comparison of Four Schemes," Computer Methods in Applied Mechanics and Engineering, Vol. 48, Feb. 1985, pp. 1-24.

[13] Turan, A. and VanDoormal, J. P., "Improved numerical methods for turbulent viscous recirculating flows," NASA CR 180852, 1987.

[14] Korczak, K. Z. and Hu, D.,"Turbulent Mixing Layers - Direct Spectral Element Simulation," AIAA paper no. 87-0133, 1987.

[15] Bechert, D. W., "Excitation of Instability Waves," Z. Flugwiss. Weltraumforsch. 9 (1985), Heft 6.

[16] Hussain, A.K.M.F. and Zaman, K.B.M.Q.,"An experimental study of organized motions in the turbulent plane mixing layer", Journal of Fluid Mechanics, vol. 159, 1985, pp. 85-104.

[17] Claus, R.W., Huang, P.G. and MacInnes, J.M.,"Time-Accurate Simulations of a Shear Layer Forced at a Single Frequency," NASA TM 100836, 1988.

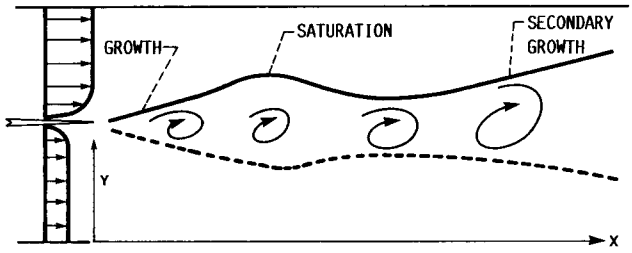

FIGURE 1. - TWO-DIMENSIONAL FLOW GEOMETRY SHOWING THE ORIENTATION OF THE AXES AND MAJOR FLOW FIELD FEATURES.

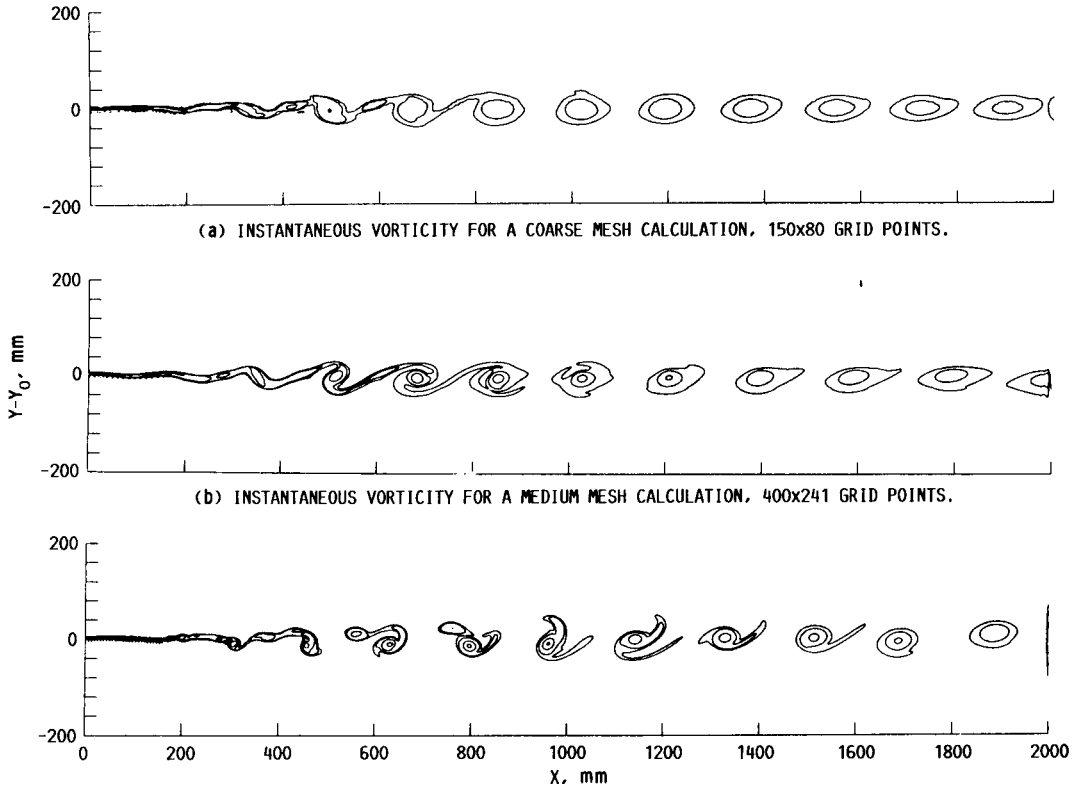

(a) INSTANTANEOUS VORTICITY FOR A COARSE MESH CALCULATION, 150x80 GRID POINTS.

(b) INSTANTANEOUS VORTICITY FOR A MEDIUM MESH CALCULATION, 400x241 GRID POINTS.

(c) INSTANTANEOUS VORTICITY FOR A FINE MESH CALCULATION, 798x241 GRID POINTS.

FIGURE 2. - INSTANTANEOUS VORTICITY CONTOURS FOR LARGE EDDY SIMULATIONS OF VARIOUS MESH DENSITIES. CONTOURS OF -500, -100, -50 AND DASHED +50.

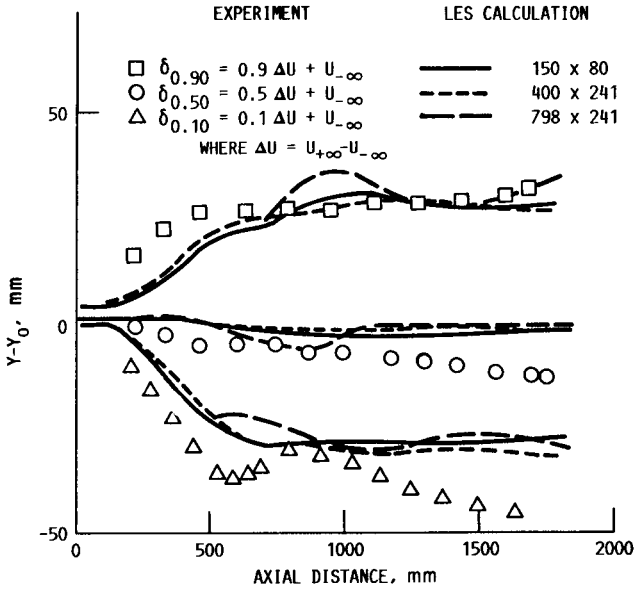

FIGURE 3. - COMPARISON OF EXPERIMENTALLY MEASURED AND CALCULATED MEAN AXIAL VELOCITY THICKNESS.

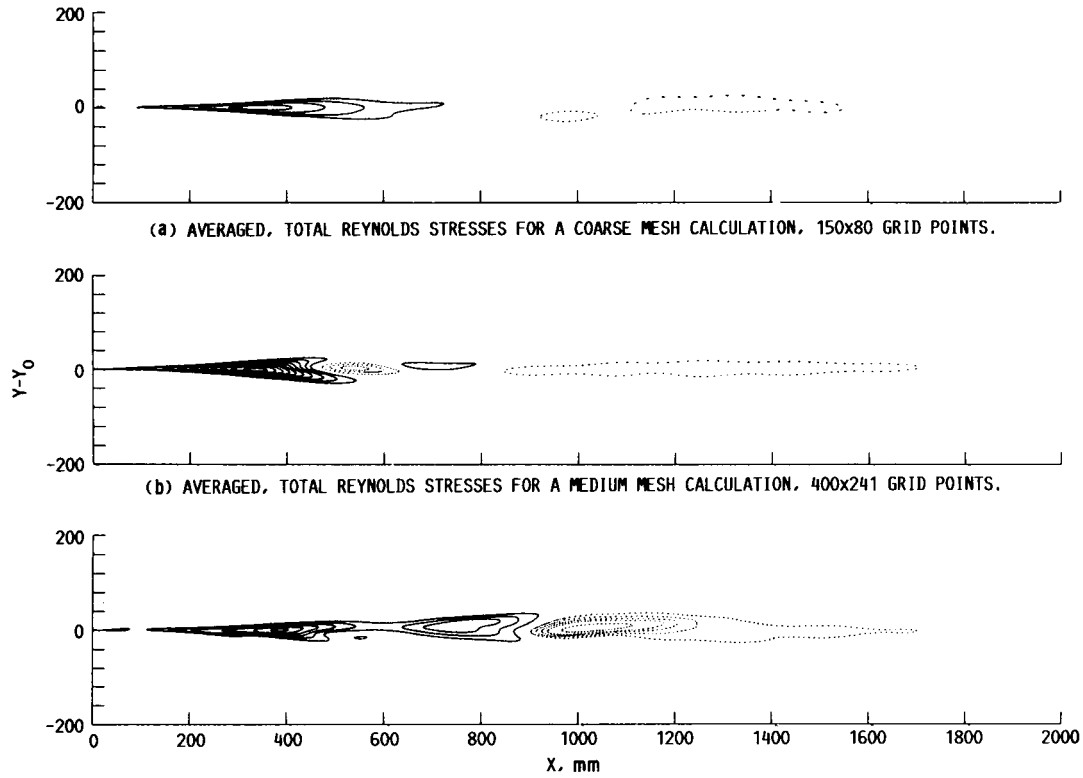

(a) AVERAGED, TOTAL REYNOLDS STRESSES FOR A COARSE MESH CALCULATION, 150x80 GRID POINTS.

(b) AVERAGED, TOTAL REYNOLDS STRESSES FOR A MEDIUM MESH CALCULATION, 400x241 GRID POINTS.

(c) AVERAGED, TOTAL REYNOLDS STRESSES FOR A FINE MESH CALCULATION, 798x241 GRID POINTS.

FIGURE 4. - AVERAGED TOTAL REYNOLDS STRESSES ($-\overline{uv}/\Delta U^2$) FOR LARGE EDDY SIMULATIONS OF VARIOUS MESH DENSITIES. CONTOURS RANGE FROM: SOLID LINES, 0.0075 TO 0.0750 IN INCREMENTS OF 0.0075 AND DASHED LINES, -0.0300 TO -0.0075 IN INCREMENTS OF 0.0075.

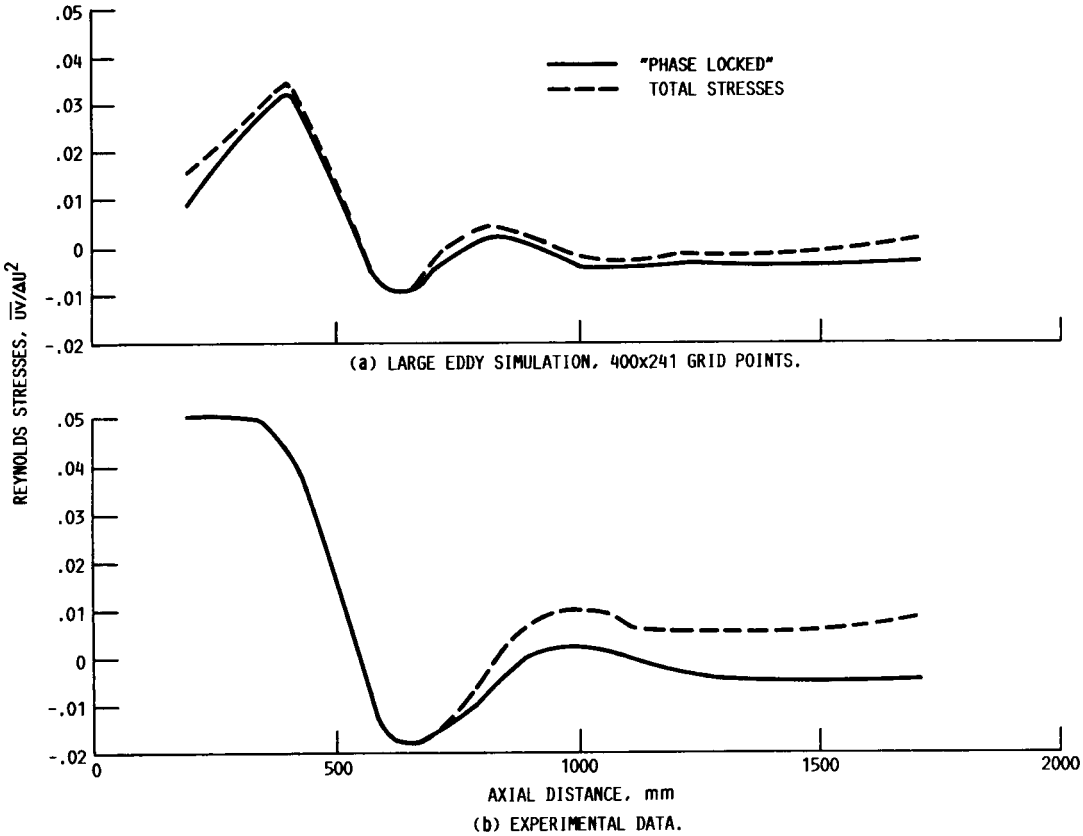

(a) LARGE EDDY SIMULATION, 400x241 GRID POINTS.

(b) EXPERIMENTAL DATA.

FIGURE 5. - CENTERLINE ($Y - Y_0 = 0$ mm) "PHASE LOCKED" AND TOTAL REYNOLDS STRESSES AS A FUNCTION OF AXIAL DISTANCE.

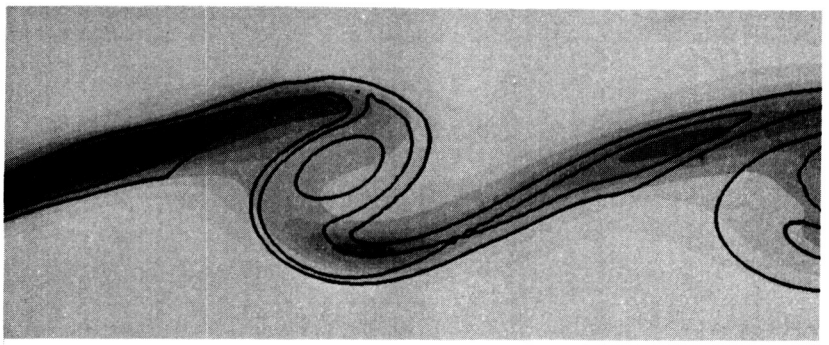

(a) MEDIUM MESH CALCULATION, EARLY IN THE FLOW DEVELOPMENT.

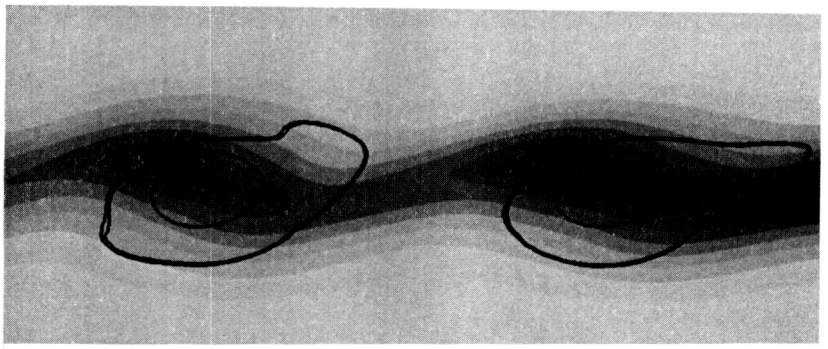

(b) MEDIUM MESH CALCULATION, NEAR THE OUTFLOW BOUNDARY.

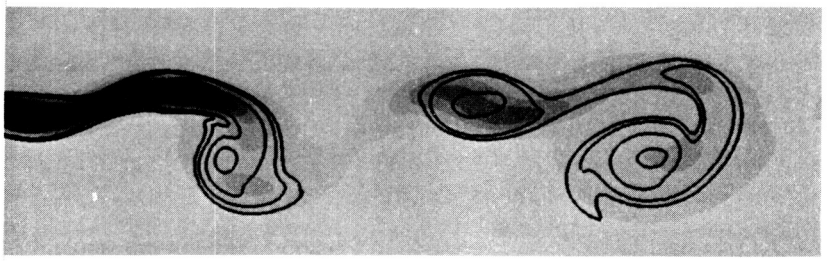

(c) FINE MESH CALCULATION, EARLY IN THE FLOW DEVELOPMENT.

FIGURE 6. - INSTANTANEOUS VORTICITY CONTOURS SUPERIMPOSED ON A GREY SCALE REPRESENTATION OF THE TURBULENCE MODEL KINETIC ENERGY, DARKER COLORS INDICATE HIGHER LEVELS OF KINETIC ENERGY.

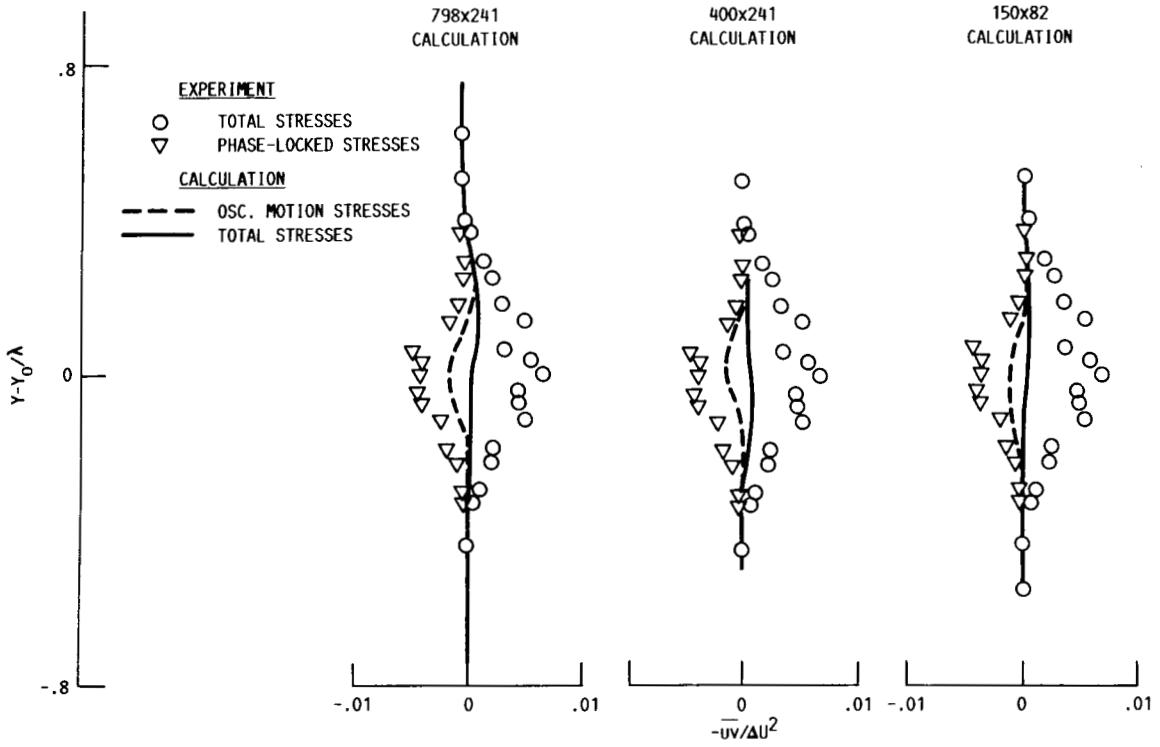

FIGURE 7. - TOTAL AND "PHASE LOCKED" REYNOLDS TRESSES, EXPERIMENTALLY MEASURED AT X = 1700 mm, COMPARED WITH THREE LARGE EDDY SIMULATIONS. λ = FORCING WAVELENGTH.

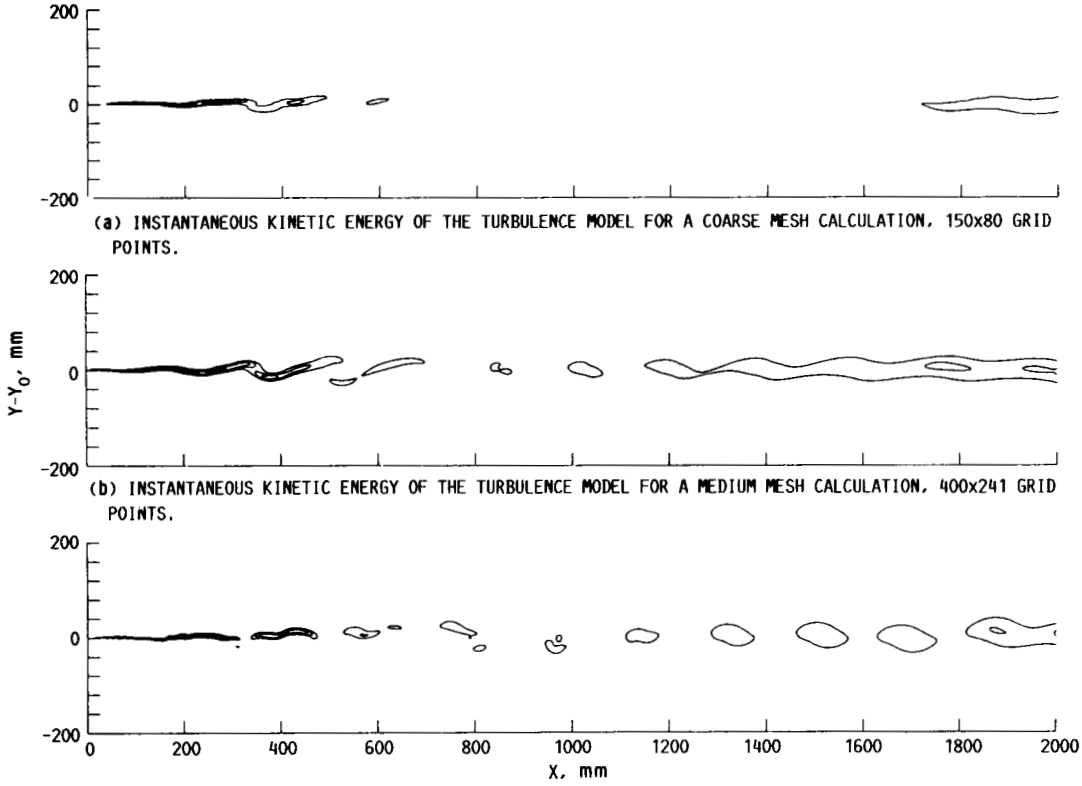

(a) INSTANTANEOUS KINETIC ENERGY OF THE TURBULENCE MODEL FOR A COARSE MESH CALCULATION, 150x80 GRID POINTS.

(b) INSTANTANEOUS KINETIC ENERGY OF THE TURBULENCE MODEL FOR A MEDIUM MESH CALCULATION, 400x241 GRID POINTS.

(c) INSTANTANEOUS KINETIC ENERGY OF THE TURBULENCE MODEL FOR A FINE MESH CALCULATION, 798x241 GRID POINTS.

FIGURE 8. - INSTANTANEOUS TURBULENCE MODEL KINETIC ENERGY FOR THREE LARGE EDDY SIMULATIONS. $K/\Delta U^2$ = 0.6 TO 4.2 INCREMENTS OF 0.6.

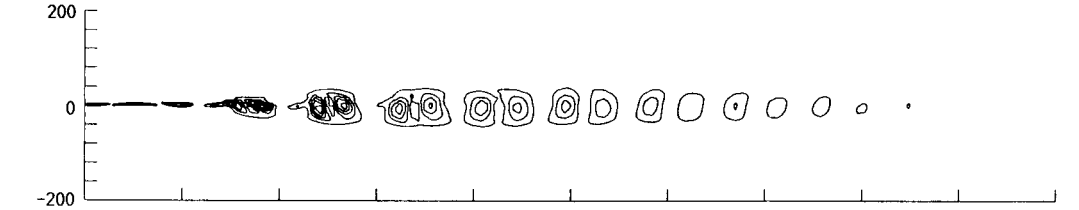

(a) INSTANTANEOUS KINETIC ENERGY OF THE OSCILLATORY MOTION, 150x80 GRID POINTS.

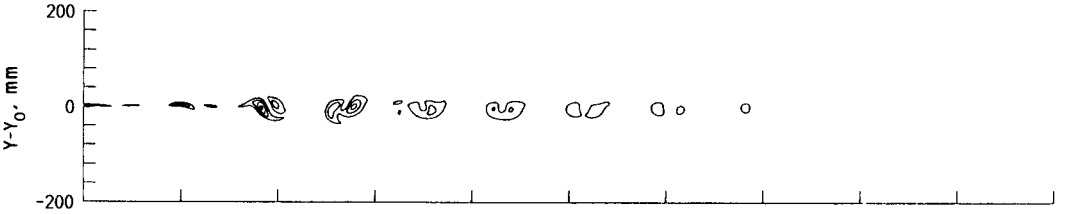

(b) INSTANTANEOUS KINETIC ENERGY OF THE OSCILLATORY MOTION, 400x241 GRID POINTS.

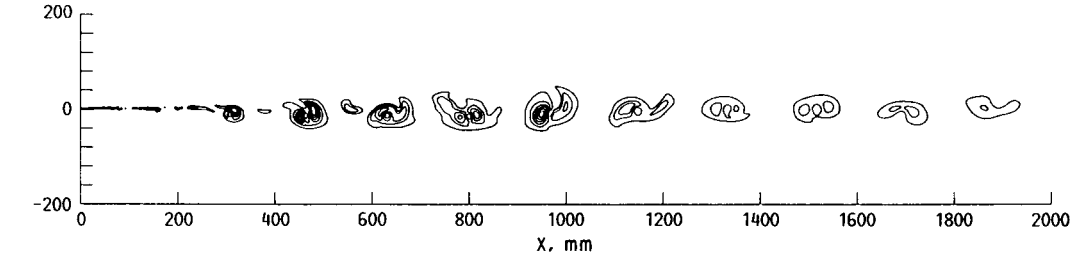

(c) INSTANTANEOUS KINETIC ENERGY OF THE OSCILLATORY MOTION, 798x241 GRID POINTS.

FIGURE 9. - INSTANTANEOUS KINETIC ENERGY OF THE OSCILLATORY MOTION FOR THREE LARGE EDDY SIMULATIONS OF VARIOUS MESH DENSITIES. $K/\Delta U^2$ = 3.0 TO 18.0 IN INCREMENTS OF 3.0.

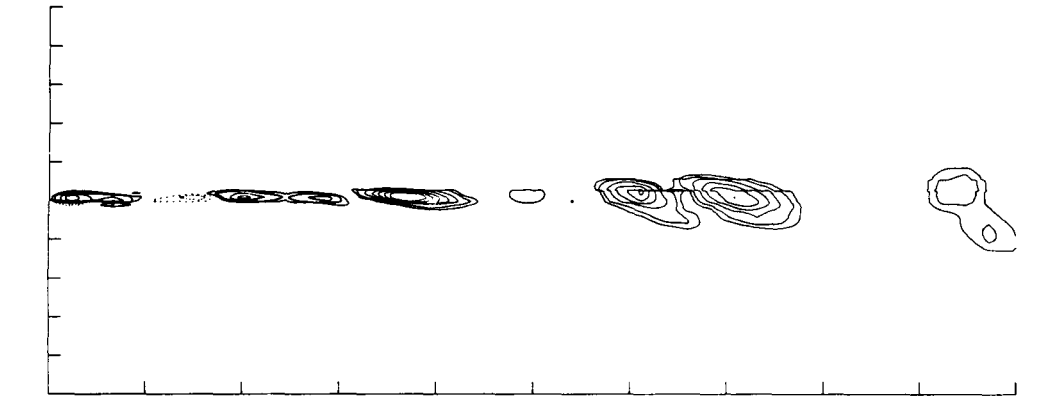

(a) COARSE MESH RESULTS. CONTOUR LEVELS: NEGATIVE (DASHED), -0.01 TO -0.04 IN INCREMENTS OF 0.01, POSITIVE (SOLID), 0.005 TO 0.070 IN INCREMENTS OF 0.005.

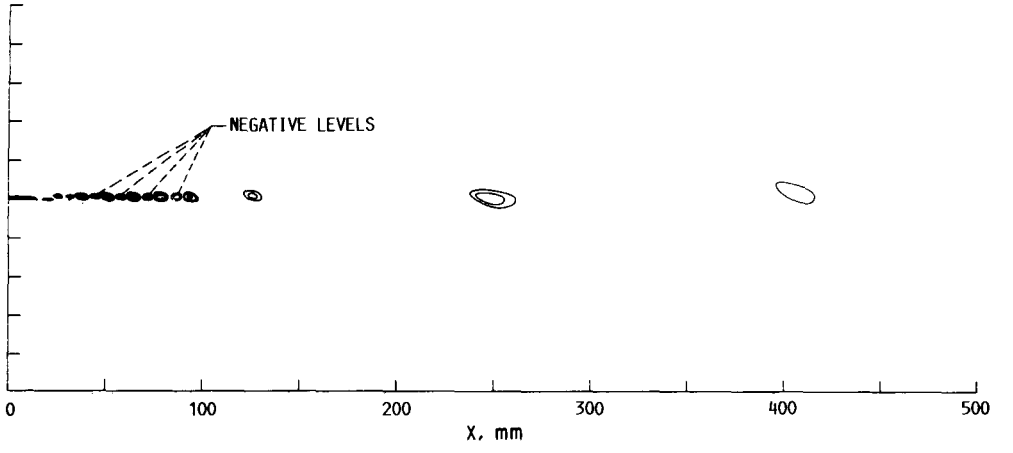

(b) FINE MESH RESULTS. CONTOURS LEVELS: NEGATIVE (DASHED), -0.4 TO -0.1 IN INCREMENTS OF 0.1, POSITIVE (SOLID), 0.05 TO 0.50 IN INCREMENTS OF 0.05.

FIGURE 10. - MAGNITUDE AND LOCATION OF GENERATION TERMS FOR OSCILLATORY MOTION KINETIC ENERGY BY THE MEAN VELOCITY GRADIENTS.

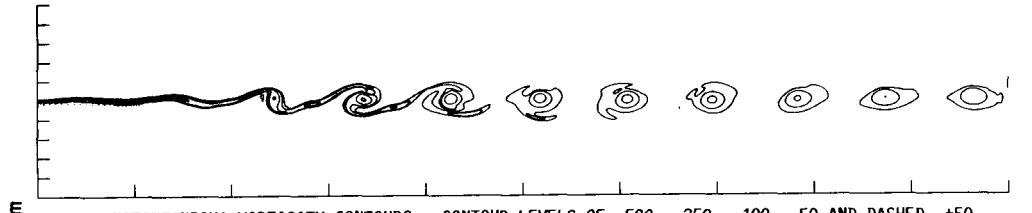

(a) INSTANTANEOUS VORTICITY CONTOURS. CONTOUR LEVELS OF -500, -250, -100, -50 AND DASHED, +50.

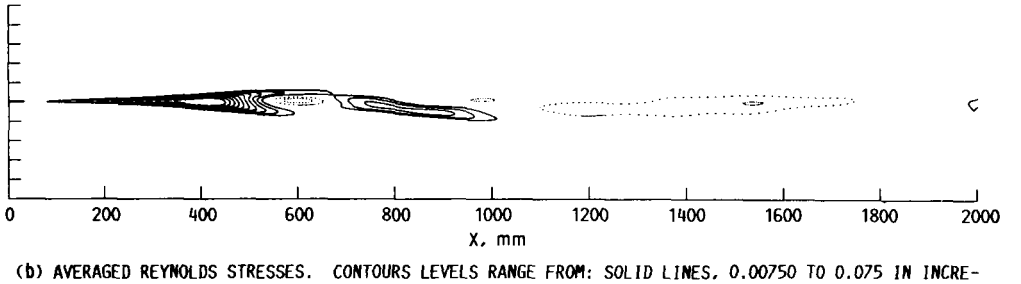

(b) AVERAGED REYNOLDS STRESSES. CONTOURS LEVELS RANGE FROM: SOLID LINES, 0.00750 TO 0.075 IN INCREMENTS OF 0.0075 AND DASHED, -0.030 TO -0.0075 IN INCREMENTS OF 0.0075.

FIGURE 11. - RESULTS OF A LAMINAR CALCULATION (Re = 9600) USING 400x241 MESH POINTS.

NASA
National Aeronautics and Space Administration

Report Documentation Page

1. Report No.	2. Government Accession No.	3. Recipient's Catalog No.
NASA TM-102129		

4. Title and Subtitle	5. Report Date
Mesh Refinement in a Two-Dimensional Large Eddy Simulation of a Forced Shear Layer	June 1989
	6. Performing Organization Code

7. Author(s)	8. Performing Organization Report No.
R.W. Claus, P.G. Huang, and J.M. MacInnes	E-4844
	10. Work Unit No. 505-62-21

9. Performing Organization Name and Address	11. Contract or Grant No.
National Aeronautics and Space Administration Lewis Research Center Cleveland, Ohio 44135-3191	
	13. Type of Report and Period Covered Technical Memorandum

12. Sponsoring Agency Name and Address	14. Sponsoring Agency Code
National Aeronautics and Space Administration Washington, D.C. 20546-0001	

15. Supplementary Notes

R.W. Claus, NASA Lewis Research Center; P.G. Huang, Stanford University, Stanford, California; and J.M. MacInnes, Princeton University, Princeton, New Jersey.

16. Abstract

A series of large eddy simulations are made of a forced shear layer and compared with experimental data. Several mesh densities were examined to separate the effect of numerical inaccuracy from modeling deficiencies. The turbulence model that was used to represent small scale, three-dimensional motions correctly predicted some gross features of the flow field, but appears to be structurally incorrect. The main effect of mesh refinement was to act as a "filter" on the scale of vortices that developed from the inflow boundary conditions.

17. Key Words (Suggested by Author(s))	18. Distribution Statement
Large eddy simulation Excitation Turbulence	Unclassified – Unlimited Subject Category 34

19. Security Classif. (of this report)	20. Security Classif. (of this page)	21. No of pages	22. Price*
Unclassified	Unclassified	20	A03

*For sale by the National Technical Information Service, Springfield, Virginia 22161